Depletion of glycosaminoglycans decreases contact stiffness of single collagen I fibrils in aqueous solution

Jonathan Roth,[a] Cody L. Hoop,[a] Jonathan K. Williams,[a] Robert Hayes,[*a] and Jean Baum [*a]

a) Department of Chemistry and Chemical Biology, Rutgers, The State University of New Jersey, Piscataway, NJ 08854. E-mail: jean.baum@rutgers.edu or rob.hayes@rutgers.edu

Abstract

Collagen fibrils serve as the molecular scaffolding for connective tissues throughout the human body and are the most abundant protein building block in the extracellular matrix (ECM). Glycosaminoglycans (GAGs) are an important class of polysaccharides in the ECM that mediate collagen fibril development, cell adhesion and motility, wound healing, inter alia. Depletion or mis-regulation of GAGs has been shown to be intimately related to diseases such as cancer, hyperglycemia, and glaucoma. However, the molecular-level coordination between collagen fibrils and GAGs to regulate ECM mechanobiology is unclear. Here, high resolution atomic force microscopy experiments are used to assess perturbations to nanoscale topography and mechanical properties of single collagen fibrils upon GAG depletion in aqueous solution. Fast force maps show that GAG depletion lowers indentation modulus by about half compared to native fibrils while retaining a key structural motif (D-banding). These results shed new light on the functional role of GAGs and may aid in strategies to treat diseases that impair ECM mechanobiology.

Introduction

Fibrilliar collagen has many important structural and functional roles in the human body.[1] Its interactions with molecular partners are significant for homeostatic function[2-4] and many are sensitive to the ECM mechanobiology, which when misregulated may lead to a number of diseases.[3, 5, 6] For example, increased stiffness may contribute to tumor cell proliferation.[5] Recently, much scientific interest has focused on understanding the mechanisms by which the ECM orchestrates the mechanics of constituient collagen fibrils.[7] However, this is complicated in part by the hierarchy of length scales of collagen self-assembly (*c.f.* Figure 1a) from single fibrils to tendon to macro-scale tissues (which may in turn exhibit different stress–strain relationships) as well as the lack of direct probing techniques under physiological conditions.[1, 8, 9] In order to gain fundamental insight into ECM function, new basic knowledge of the mechanics of single collagen fibril building blocks is required.

The highly conserved collagen assembly is regulated by proteoglycans (PGs), in which protein cores are bound to anionic polysaccharide chains, called glycosaminoglycans (GAGs).[10, 11] A large diversity of PGs and GAGs are distributed across connective tissues for proper ECM activity.[10] In all tissues, PGs recognize a number of specific amino acid sequence motifs on collagen fibrils[12-15] to act as part of the ECM scaffolding (Figure 1a). However, their specific structural roles have been debated. They have been proposed to form fibril–fibril crosslinks within higher order fibril bundles, or fibers, to in turn regulate load bearing.[16] In contrast, the hydrophilic GAG chains may not couple individual fibrils, but rather isolate them to enable fibril sliding under load and preserve fiber structural integrity.[17]

In addition to their structural roles, GAGs have been shown to be essential for wound healing, cell adhesion, and cell motility.[10, 18, 19] As such, depletion or misregulation of GAGs is often associated with natural aging[20] or debilitating diseases.[21-23] Notably, it has been proposed that misregulation of GAGs perturbs the mechanobiology of the ECM, leading to a loss of biological function and aberrant cell activity.[7] However, the mechanism and extent to which GAGs alter individual collagen fibrils has not been elucidated.

Here, we investigate the influence of GAG content on individual collagen fibrils in aqueous buffer solution via atomic force microscopy (AFM) experiments. AFM is a powerful and versatile experimental technique in biophysics. Recently, the emergence of sophisticated AFM-imaging modes has enabled direct, high resolution pictures of structure or mechanical / surface properties of biological systems *in situ* under physiological aqueous conditions.[24, 25] For collagen, many AFM papers have confirmed the characteristic D-banding every ~67 nm of adsorbed fibrils.[26-31] However, these studies have largely been restricted to measurements in air, which itself complicates imaging due to trace water. Given that most collageneous tissue functions in a fully hydrated environment, its interaction in water with small molecules such as GAGs is of paramount importance. In this study, two advanced AFM imaging modes are used to study the association of GAGs with collagen fibrils derived from rat tail tendons in aqueous solution. First, amplitude-modulation (AM-) AFM experiments resolve the characteristic

D-banding and hydrated nanostructure. Second, complementary fast force mapping (FFM-) AFM experiments examine how GAGs alter individual collagen fibril mechanics in nanoscale space in aqueous solution. Together, these results present a molecular-level picture of GAG–collagen fibril interactions under physiological conditions.

Results and Discussion

Resolving collagen fibril D-banding in solution.

Collagen fibrils display a canonical D-banding pattern every 67 nm that is produced by the staggered arrangement of triple helical tropocollagen units[9] (Figure 1a). In Figure 1b-c, AM-AFM confirms such banding is present in rat tail collagen fibrils adsorbed to a glass slide, whether measured in air or immersed in PBS buffer solution. Here, the sinusoidal periodicity in the height along the main fibril axis is observed in both imaging environments, with an alternating structure of a high region, *the overlap* (yellow), and low region, *the gap* (orange-red). Despite slight reduction in image clarity in solution compared to air, D-banding periodicity was maintained, measuring 65.2 ±1.4 nm (N=5) versus 66.0 ±0.5 nm (N=2), respectively (Figure 1b, S1a,b) by Fourier transform. This provides a structural basis to explain changes in nanomechanical properties.

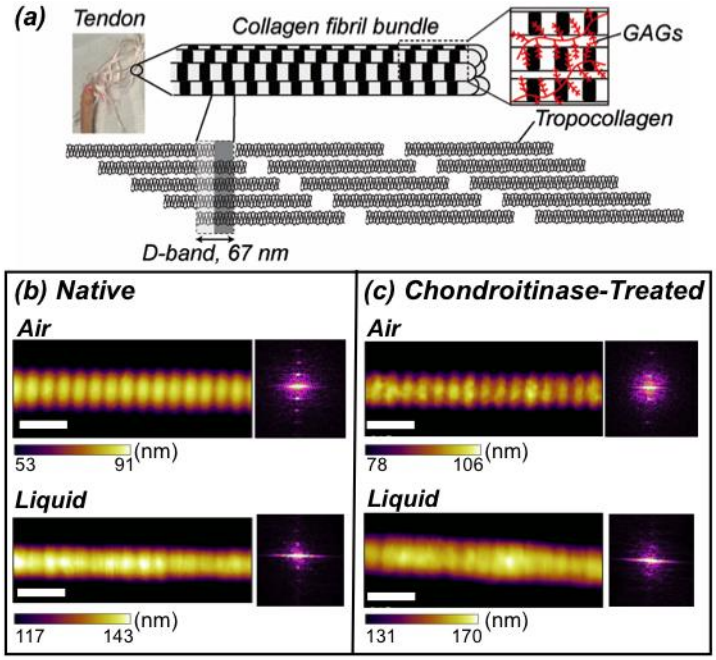

Figure 1. Collagen fibril D-banding. (a) Schematic of fibrillar collagen hierarchy from rat tail tendons to triple helices. The major protein component of tendon ECM is collagen I in the form of fibril bundles, or fibers. PGs (red) displaying GAGs interact with individual fibrils within a fibril bundle. The characteristic D-bands are produced by the staggered arrangement of triple helical tropocollagens, resolved here by AM-AFM experiments for both (b) native and (c) chondroitinase-treated collagen fibrils imaged in air and liquid environments. The white scale bars are 200 nm in each image. The Fourier transform insets show the periodicity of each fibril. Uncropped height, amplitude, and phase images are shown in the ESI (Figure S2).

One important consideration between data in air and solution is the effect of fibril hydration. This can be assessed by measuring the average height along the apex of the

fibril surface and taking the ratio of height in solution relative to that in air. For native fibrils, the ratio factor is estimated to be 1.79 ± 0.06 (N=5), confirming swelling in solution. This suggest a radial enlargement due to entrained water, consistent with previous measurements on collagen[32] or other fibriliar units[33].

D-banding is maintained upon depletion of GAGs.

We next investigated the structural effect of GAG depletion. The chondroitinase treated fibirls presented here have a 76% reduction in GAG content compared to native counterparts as measured using standard assays.[34] Image analysis of AFM data in Figure 1c show that treated fibrils display D-bands every 66.2 ± 0.4 nm in air (N=5) and 66.0 ± 0.1 nm in PBS solution (N=3). This is in excellent agreement with the native fibril data (Figure 1b) and for AFM results of chondroitinase treated tendons in air.[17] Likewise, the step height between overlap–gap regions in liquid is found to be 2.2 ± 0.9 nm in native fibrils (N=5) versus 3.0 ± 0.9 nm upon treatment (N=4). Finally, GAG-depleted fibrils have a swelling factor of 1.9 ± 0.2 (N=5). Overall, the data show that not only is fibril *periodicity* maintained, but the *topography* and *hydrated structure* are essentially invariant on GAG association. This indicates that collagen fibril nanoscale structure is preserved upon GAG depletion in aqueous solution.

AFM force mapping reveals a decreased indentation modulus of individual collagen fibrils upon GAG depletion.

FFM-AFM was used to measure the local nanoscale contact stiffness of individual collagen fibrils in solution in both states. Figure 2 presents a 1 x 1 μm force map of native and GAG-depleted collagen fibrils, respectively. Unlike in Figure 1, it is important to emphasize that these images are 2D maps of contact force at each pixel, corrected using standard protocols[59] into indentation moduli (Fig. S3). This enables mechanical data to be compared to the structural data on the nanoscale.

Notably, D-banding is evident in both force maps; the overlap region is systematically lighter than the gap regions, leading to a distinct light/dark/light patterning ~67 nm down the long axis. While the demarcation between gap/overlap is less well-defined than for AM- data, the results show that even in solution, collagen mechanics oscillate on the nanoscale as prescribed by the underlying D-banded structure. Specifically, the staggered arrangement of monomer units leads to more elastic gap compared to overlap regions due to the reduced molecular density. Similar conclusions were previously reported for untreated hydrated collagen fibrils.[58]

Untreated and treated collagen fibrils display important differences in the force maps. Significant reduction in average local indentation modulus is evident. In Figure 2a, overlap regions are red on the native fibril (~9 MPa) compared to light blue (~5 MPa) for treated fibrils. Likewise, corresponding gap regions shift from yellow (~7 MPa) to dark blue (~2 MPa) upon treatment while preserving the native D-banded structure.

To better understand these differences, and exclude data that may be contaminated by biological debris introduced upon chondrotiniase treatment, we focused on the 256 force

curves down the apex of each fibril (Figure 2c). The native, untreated collagen fibrils exhibit a mean indentation modulus of 6.4 ±1.4 MPa with a broad distribution of values over the fibrils measured (Figure 2a, c, S4). This is consistent with reported moduli of collagen fibrils with similar indentation speeds.[31] For treated fibrils, both the average indentation modulus (2.9 ±1.0 MPa) and data range is reduced (Figure 2b, c, S4). This again indicates that GAGs reduce fibril stiffness on the nanoscale.

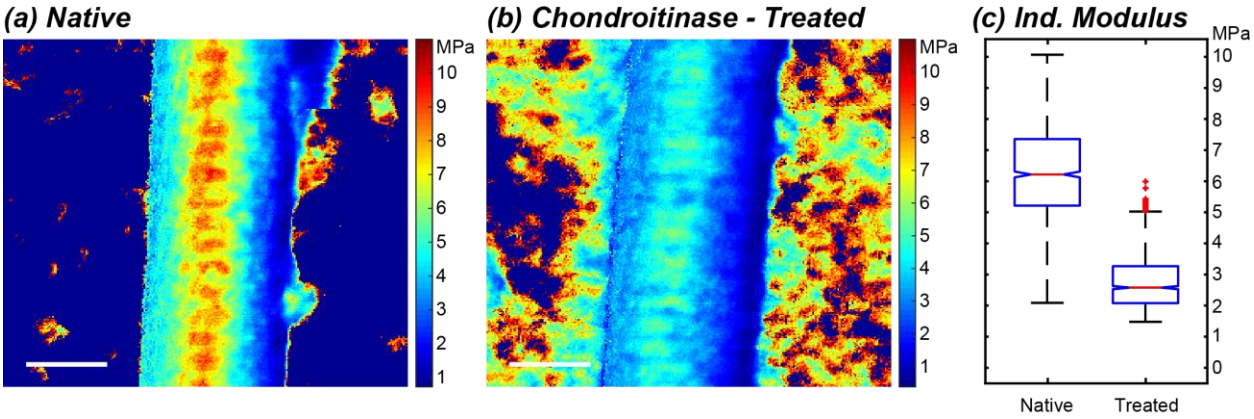

Figure 2. Nanoscale indentation modulus maps of collagen fibrils in solution. (a,b) Representative 1 x 1 μm fast force maps of individual (a) native, untreated and (b) chondroitinase-treated, GAG-depleted collagen fibrils from FFM-AFM experiments. The color at each pixel shows the *local* nanoscale indentation modulii (1 pixel / every ~15 nm^2); the FFM images are spatial reconstructions of 65,536 discrete force–distance curves that were fitted using standard indentation protocols[35] and subsequently replotted in Cartesian space using in-house MATLAB code. A large scan size was selected to capture more than ten D-bands per image, enabling meaningful comparisons between internal regions, fibrils, and treatments. White scale bars indicate 200 nm. (c) Box and whisker plots compare a subset of indentation moduli data in (a) and (b) for force curves acquired only at the apex down the fibril long axes. In (c), data for five fibrils in each condition are presented for increased statistical confidence.

How does GAG depletion affect nanomechanics within the D-band? To assess this, an overlap/gap indentation modulus ratio was estimated for D-bands in native and treated fibrils by taking the ratio of indentation moduli of overlap regions relative to neighboring gap regions. In native fibrils, this was determined to be 1.3 ± 0.1 from analysis of data in Figure 2a. This is consistent with a reported 20% increase in the ratio when measured in air,[36] attributed to the higher tropocollagen density in the overlap relative to the gap defined in the Hodge–Petruska model[9, 31] (Figure 1a). Here, no change in the overlap/gap indentation of treated fibrils is observed as the modulus ratio remains invariant at 1.3 ± 0.1. This reveals that while GAG depletion lowers the mean indentation modulus across the whole fibril, on the nanoscale both gap and overlap regions are equally affected. This is consistent with GAG-decorated PGs maintaining specific binding motifs in both the gap and overlap regions of collagen I. For example, interaction domains for dermatan and chondroitin sulfate PGs are in the gap region, while keratan and heparan sulfate PGs associate with the overlap region.[12-15, 37]

Impact of GAG-depletion on collagen fibril mechanics.

From these experiments, it is possible to draw broader conclusions about how GAGs mediate collagen mechanics. First, it is important to note that the observed changes in nanomechanics are expressed uniformly on the collagen fibril, due to depletion of GAGs

from PGs interacting with motifs in both the gap and overlap regions. In solution, the negatively charged GAGs may attract ions (or water molecules) to induce an osmotic pressure near the fibril surface.[38, 39] Osmotic pressure has long been suggested to play a role in collagen tensile strength in physiological conditions.[19, 40] This type of structural change in solution would serve to effectively compress collagen fibrils, explaining the higher measured indentation modulus in the case of the native collagen fibrils relative to the GAG-depleted fibrils in Figure 2. However, the absence of changes in swelling factor indicates that water is not the dominant player here. Rather, the decreased indentation modulus leads us to propose that the osmotic pressure changes are driven chiefly by ionic associations of the GAGs with the collagen fibril. We further note that collagen is highly susceptible to contraction upon interactions with ions; for example, some of the first molecular machines exploited this effect[41]. In reality, there is likely both water and complex specific-ion effects[42] at very small length and time scales, currently beyond the resolution of the instrument.

Because fibrils are the building blocks of high-order collagen structures, these results have important implications for the behavior of macroscopic tissues such as fibres and tendons. However, to date, there is still no consensus on the impact of GAG content on macroscopic tissue tensile properties.[17, 43-48] A reduction in GAGs have been shown to have no effect on elastic properties of tendons[17, 46, 47] yet can modulate tendon integrity.[49, 50] In a tendon injury model, increased GAG levels due to the injury was shown to reduce the elastic modulus of the injured tendons, and this could be partially rescued by chondroitinase ABC treatment.[43] For other collagenous tissues, such as placenta[44] and sclera,[45] GAG depletion was correlated to a reduction of tensile strength, as we observe for individual fibrils. Further complicating the issue, the moduli of soft biological tissues are sensitive to the probe itself (e.g. deformation by indentation vs. tensile measurement).[51] This suggests that GAG depeletion in collagen is complex and tissue-specific, and there are likely different and possibly competing mechanism/s operating at different length scales.

The mechanical properties of single collagen fibrils can be modulated by chemical environment,[27, 52, 53] temperature,[31, 52] hydration,[30, 32] UV exposure,[52] and sugars that induce advanced glycation end-products.[54] This highlights the biomechanical sensitivity of the fibril building blocks to external factors. AFM has been the primary tool for force measurements on biological systems, given its resolution on nanometer length scales and its utility in physiological liquid environments. In this study, using advanced AFM protocols, we have shown that the contact stiffness of individual collagen fibrils is reduced in GAG depleted tendons in a non-localized manner on the nanoscale, which may contribute to reduced cell functionality with natural aging or in GAG-depleted disease states.

Conclusions

It is increasingly clear that alteration of GAG concentration is intimately associated with the progression of aging and diseases that cause destruction in numerous connective tissues. Here, we show that under physiological solution conditions, GAG depletion

decreases stiffness of individual collagen fibrils while maintaining their native nanoscale topography. We expect that mechanical properties at the fibril hierarchy will influence the mechanobiology of the ECM, and mechanical decline may compromise cell–ECM interactions and reliant cell processes, which may play a role in aging and disease progression. Still, further research will be required to make a direct association between GAG depletion and cell activity or how the effect operates at longer length scales beyond the fibril building block. We now have a greater understanding of the effects of GAG depletion on collagen fibril stiffness, which could aid in development of new treatment strategies for diseases associated with ECM mechanobiology.

Materials and Methods

Preparation of collagen fibril samples and chondroitinase treatment: Rat tail tendons were harvested from frozen–thawed rat tails. Chondroitinase treatment of tendons was performed in a similar manner to previously published methods.[17] In short, sections of tendon several centimeters in length were cut from the exposed tail tendons. For chondroitinase treatment, the tail tendon sections were placed into a 4 mL solution of 0.15 U/mL chondroitinase ABC (Sigma-Aldrich) in 0.1 M sodium acetate and 0.1 M Tris-HCl, pH 8. For the untreated control, fibrils were placed in the same buffer in the absence of chondroitinase. These are referred to as native fibrils. The tendons were incubated in this solution at 37°C overnight. Afterwards, the tendon sections were rinsed with fresh PBS buffer solution (pH 7.4) and smeared onto a microscope glass slide in order to deposit a film of collagen fibrils onto the surface. Prior to experiments, microscope glass surfaces were sonicated in ultrapure water, rinsed with ethanol, and then dried with ultra-high purity nitrogen. The samples were then washed with ultrapure water and allowed to dry for one hour in a laminar flow hood (1300 Series A2, Thermo Scientific). Once dry, a stereoscope was used to locate and assess fibril deposition prior to AFM experiments.

Quantification of GAG depletion: Sections of separately prepared rat tail tendon were weighed, and then given the same chondroitinase/control treatment provided above. Tendons were then rinsed with water and placed into 1 mL of a papain solution (500 µg papain, 0.1 M dibasic sodium phosphate, 0.144 M EDTA, 0.1 M L-cysteine) at 60°C for 24 hours to digest the tendons. The resulting solution was stained with dimethylmethylene-blue and absorbance was measured at 525 nm. A standard curve of varying chondroitin sulfate concentrations (0.25–1.5 µg/mL) was used to quantify the GAG concentration in the treated and control samples.

Atomic force microscopy (AFM): Amplitude modulation (AM-) imaging and fast force mapping (FFM-) experiments were performed on a Cypher ES AFM (Asylum Research, Oxford Instruments). Silicon nitride cantilevers AC240 and Biolever-mini BL-AC40TS sourced from Oxford Instruments were used for AM imaging in air and liquid, respectively. These cantilevers have a nominal spring constant of kc = 2.0 Nm^{-1} and 0.1 Nm^{-1}, and radii of r = 7 nm and 8 nm, respectively. Image and force measurements were acquired at 25°C. The glass microscope slide surface with deposited collagen fibrils was mounted on a steel puck within the AFM box (a sealed enclosure). Samples were first imaged in air to locate and characterize the collagen fibrils. Before liquid experiments, the spring constant of the cantilever was first determined in air using the GetReal function in the Asylum Research AFM software, which is a combination of the Sader[55] and thermal noise methods. The inverse optical lever sensitivity (InVOLS) was then determined by averaging the results of ten force curves on a sapphire surface in PBS buffer.

Liquid experiments were completed in a droplet of approximately 0.25 mL of fresh 10 mM PBS buffer, pH 7.4 solution on the glass microscope slide surface at 25°C. To minimize thermal drift, this setup was allowed to equilibrate for at least one hour in the AFM prior to imaging. To facilitate obtaining high quality AM images in liquid conditions, the tip was photothermally excited at its resonance frequency using blueDrive (Asylum Research, Oxford Instruments). AFM images were analyzed using the Asylum Research AFM software and Gwyddion software.[56] To calculate the swelling ratio, the average height along the apex of a fibril in liquid was divided by the average height of the same fibril in air. For determination of the overlap–gap step height from the AM images, the minimum height of a gap region was subtracted from the maximum height of the neighboring overlap region (Figure S1). For each overlap, the average step height from two neighboring gaps was taken. FFM experiments were performed immediately following AM-AFM imaging on the same fibrils characterized in air and liquid. The same BL-AC40TS AFM probe as referenced above was used for all nanoindentation experiments. Force maps were acquired at a scan size of 1 µm x 1 µm with a pixel resolution of 256 x 256 points, a scan rate of 20 Hz and a setpoint of 2 nN. The indentation moduli of the fibrils were then determined from the force maps produced using the analysis of the matrix of force curves as described below.

Post-Processing Analysis: FFM data sets were analyzed using custom in-house Matlab (R2018b) scripts. In brief, indentation moduli were calculated for each force curve iteratively using the methods detailed by Andriotis and coworkers.[35] The resulting 256x256 matrix of FFM indentation moduli was then reconstructed in Cartesian space as a scaled colormap (Figure 2a–b). Box and whisker plots were derived from a subset of five FFM images for each treatment. Here, force curve data at the height apex along the fibril longitudinal axis was extracted (256 moduli), and pooled among treatments. For this study, the apex corresponds to the values along a straight line created between two of the highest values at opposite ends of the fibril. A one-way analysis of variance (ANOVA) was performed, and the moduli data from each treatment condition are shown as a boxplot in Figure 2c. A similar method as described for the step height was used to determine the overlap/gap indentation modulus ratios from the FFMs (Figure S4).

Conflicts of interest

There are no conflicts to declare.

Acknowledgements

This work was supported by NIH grant GM045302 to JB and an Exploratory Research Seed Grant from the VCRI to RH. The authors acknowledge Dr. Joseph Freeman and Michael Pellegrini for assistance with rat tail procedures.

References

1. D. F. Holmes, Y. Lu, T. Starborg and K. E. Kadler, *Curr Top Dev Biol*, 2018, **130**, 107-142.

2. K. A. Jansen, D. M. Donato, H. E. Balcioglu, T. Schmidt, E. H. Danen and G. H. Koenderink, *Biochim Biophys Acta*, 2015, **1853**, 3043-3052.
3. P. Lu, V. M. Weaver and Z. Werb, *J Cell Biol*, 2012, **196**, 395-406.
4. A. J. Engler, S. Sen, H. L. Sweeney and D. E. Discher, *Cell*, 2006, **126**, 677-689.
5. D. E. Jaalouk and J. Lammerding, *Nat Rev Mol Cell Biol*, 2009, **10**, 63-73.
6. K. R. Levental, H. Yu, L. Kass, J. N. Lakins, M. Egeblad, J. T. Erler, S. F. Fong, K. Csiszar, A. Giaccia, W. Weninger, M. Yamauchi, D. L. Gasser and V. M. Weaver, *Cell*, 2009, **139**, 891-906.
7. V. Vogel, *Annu Rev Physiol*, 2018, **80**, 353-387.
8. F. H. Silver, J. W. Freeman and G. P. Seehra, *J Biomech*, 2003, **36**, 1529-1553.
9. J. A. Petruska and A. J. Hodge, *Proc Natl Acad Sci U S A*, 1964, **51**, 871-876.
10. C. N. M. Ryan, A. Sorushanova, A. J. Lomas, A. M. Mullen, A. Pandit and D. I. Zeugolis, *Bioconjugate Chemistry*, 2015, **26**, 1237-1251.
11. N. S. Gandhi and R. L. Mancera, *Chem Biol Drug Des*, 2008, **72**, 455-482.
12. J. P. Orgel, A. Eid, O. Antipova, J. Bella and J. E. Scott, *PLoS One*, 2009, **4**, e7028.
13. S. M. Sweeney, C. A. Guy, G. B. Fields and J. D. San Antonio, *Proc Natl Acad Sci U S A*, 1998, **95**, 7275-7280.
14. J. D. San Antonio, M. J. Karnovsky, S. Gay, R. D. Sanderson and A. D. Lander, *Glycobiology*, 1994, **4**, 327-332.
15. J. E. Scott and R. W. Glanville, *Biochem Soc Trans*, 1993, **21**, 123S.
16. N. Sasaki and S. Odajima, *J Biomech*, 1996, **29**, 1131-1136.
17. S. Rigozzi, R. Muller, A. Stemmer and J. G. Snedeker, *J Biomech*, 2013, **46**, 813-818.
18. A. R. Hackett and J. K. Lee, *Frontiers in Neurology*, 2016, **7**.
19. P. N. Lewis, C. Pinali, R. D. Young, K. M. Meek, A. J. Quantock and C. Knupp, *Structure*, 2010, **18**, 239-245.
20. E. C. Naylor, R. E. B. Watson and M. J. Sherratt, 2011, **69**, 249-256.
21. R. V. Iozzo and M. A. Gubbiotti, *Matrix Biol*, 2018, **71-72**, 1-9.
22. B. J. Murienne, M. L. Chen, H. A. Quigley and T. D. Nguyen, *J R Soc Interface*, 2016, **13**, 20160367.
23. B. Law, V. Fowlkes, J. G. Goldsmith, W. Carver and E. C. Goldsmith, *Microscopy and Microanalysis*, 2012, **18**, 22-34.
24. Y. F. Dufrene, T. Ando, R. Garcia, D. Alsteens, D. Martinez-Martin, A. Engel, C. Gerber and D. J. Muller, *Nat Nanotechnol*, 2017, **12**, 295-307.
25. M. Krieg, G. Fläschner, D. Alsteens, B. M. Gaub, W. H. Roos, G. J. L. Wuite, H. E. Gaub, C. Gerber, Y. F. Dufrêne and D. J. Müller, *Nature Reviews Physics*, 2019, **1**, 41-57.
26. M. P. Wenger, L. Bozec, M. A. Horton and P. Mesquida, *Biophys J*, 2007, **93**, 1255-1263.
27. C. A. Grant, D. J. Brockwell, S. E. Radford and N. H. Thomson, *Biophys J*, 2009, **97**, 2985-2992.
28. C. J. Peacock and L. Kreplak, *Nanoscale*, 2019, **11**, 14417-14425.
29. S. Strasser, A. Zink, M. Janko, W. M. Heckl and S. Thalhammer, *Biochem Biophys Res Commun*, 2007, **354**, 27-32.
30. M. R. Uhlig and R. Magerle, *Nanoscale*, 2017, **9**, 1244-1256.
31. S. J. Baldwin, A. S. Quigley, C. Clegg and L. Kreplak, *Biophys J*, 2014, **107**, 1794-1801.
32. O. G. Andriotis, S. Desissaire and P. J. Thurner, *ACS Nano*, 2018, **12**, 3671-3680.
33. J. O. Karlsson, M. Andersson, P. Berntsson, T. Chihani and P. Gatenholm, *Polymer*, 1998, **39**, 3589-3595.
34. V. J. Coulson-Thomas and t. ferreira, *Bio-protocol*, 2014, **4**, e1236.
35. O. G. Andriotis, W. Manuyakorn, J. Zekonyte, O. L. Katsamenis, S. Fabri, P. H. Howarth, D. E. Davies and P. J. Thurner, *J Mech Behav Biomed Mater*, 2014, **39**, 9-26.
36. C. A. Grant, M. A. Phillips and N. H. Thomson, *J Mech Behav Biomed Mater*, 2012, **5**, 165-170.
37. J. E. Scott and C. R. Orford, 1981, **197**, 213-216.
38. N. D. Broom and C. A. Poole, *Arthritis Rheum*, 1983, **26**, 1111-1119.
39. S. S. Skandalis, A. D. Theocharis, D. H. Vynios, D. A. Theocharis and N. Papageorgakopoulou, *Biochimie*, 2004, **86**, 221-229.
40. A. Masic, L. Bertinetti, R. Schuetz, S.-W. Chang, T. H. Metzger, M. J. Buehler and P. Fratzl, *Nature Communications*, 2015, **6**, 5942.
41. M. V. Sussman and A. Katchalsky, *Science*, 1970, **167**, 45-47.
42. P. Lo Nostro and B. W. Ninham, *Chemical Reviews*, 2012, **112**, 2286-2322.
43. R. K. Choi, M. M. Smith, J. H. Martin, J. L. Clarke, A. J. Dart, C. B. Little and E. C. Clarke, *J Biomech*, 2016, **49**, 2694-2701.
44. K. H. Schneider, P. Aigner, W. Holnthoner, X. Monforte, S. Nurnberger, D. Runzler, H. Redl and A. H. Teuschl, *Acta Biomater*, 2016, **29**, 125-134.
45. B. J. Murienne, J. L. Jefferys, H. A. Quigley and T. D. Nguyen, *Acta Biomater*, 2015, **12**, 195-206.
46. G. Fessel and J. G. Snedeker, *J Theor Biol*, 2011, **268**, 77-83.
47. G. Fessel and J. G. Snedeker, *Matrix Biol*, 2009, **28**, 503-510.
48. S. Rigozzi, R. Muller and J. G. Snedeker, *J Biomech*, 2009, **42**, 1547-1552.
49. K. Legerlotz, G. P. Riley and H. R. Screen, *Acta Biomater*, 2013, **9**, 6860-6866.
50. H. R. Screen, V. H. Chhaya, S. E. Greenwald, D. L. Bader, D. A. Lee and J. C. Shelton, *Acta Biomater*, 2006, **2**, 505-513.
51. C. T. McKee, J. A. Last, P. Russell and C. J. Murphy, *Tissue Eng Part B Rev*, 2011, **17**, 155-164.

52. M. Schulze, M. Rogge and R. W. Stark, *J Mech Behav Biomed Mater*, 2018, **88**, 415-421.
53. X. Pang, L. Lin and B. Tang, *Scientific Reports*, 2017, **7**, 46042.
54. O. G. Andriotis, K. Elsayad, D. E. Smart, M. Nalbach, D. E. Davies and P. J. Thurner, *Biomed Opt Express*, 2019, **10**, 1841-1855.
55. J. E. Sader, J. W. M. Chon and P. Mulvaney, *Review of Scientific Instruments*, 1999, **70**, 3967-3969.
56. D. Necas and P. Klapetek, *Cent Eur J Phys*, 2012, **10**, 181-188.